Design and Kinematics of a Novel Reconfigurable Parallel Manipulator with Kirigami-inspired Plano-Spherical Linkages and Angular Pouch Motors

Ketao Zhang*

Centre for Advanced Robotics
School of Engineering and Materials Science
Queen Mary University of London
Mile End Road, London, E1 4NS
United Kingdom
Email: ketao.zhang@qmul.ac.uk

Chen Liu

Centre for Advanced Robotics
School of Engineering and Materials Science
Queen Mary University of London
Mile End Road, London, E1 4NS
United Kingdom
Email: chen.liu@qmul.ac.uk

ABSTRACT

Drawing inspiration from kirigami, this paper first presents a crease pattern of a kirigami model which is kinematically equivalent to a Bennett plano-spherical linkage. In terms of screw theory, distinct closed-loop motion branches of the linkage is revealed. Using the Bennett plano-spherical linkage as a closed-loop subchain of kinematic limbs, this paper then introduces a new reconfigurable parallel manipulator with three hybrid kinematic limbs. Each limb of the manipulator consists of a Bennett plano-spherical linkage and a R(RR) serial chain. The constraints exerted on the platform by the hybrid limb are explored by analysing motion-screw systems of the equivalent serial kinematic limb corresponding to each motion branch of the closed-loop subchain. Motion characteristics in each motion branch of the parallel manipulator are revealed. This paper further presents a new design of inflatable bending actuator and fabricated a prototype using adhesive fabric. The actuator is integrated with 3D printed prototypes of the Bennett plano-spherical linkage and parallel manipulator for reconfiguring motion branches.

1 Introduction

Parallel manipulators with multi-loop structures in general process inherent characteristics of high stiffness and dynamic performance in comparison with serial manipulators. Such advantages lead to various successful applications of parallel manipulators such as pick and place robots and machine tools [1–3]. However, traditional parallel robots were designed to implement specific tasks thus have limit adaptability to demands of task variation due to their unique topological configuration. To address these challenges and add the capability of being able to reconfigure structure without dismounting and reassembling, parallel robots with distinct function of reconfiguring their mobility and motion mode have been extensively investigated in recent years [4–8].

*Address all correspondence to this author.

An underlying principle inducing variation of motion mode and mobility of closed-loop mechanisms, including single-loop linkage and multi-loop parallel manipulator, is the geometric constraints variation across constraint singularity of this type of mechanisms. The multi-mode motion characteristics of a parallel manipulator were first observed in study of the 3-URU DYMO [9,10], which exhibits five distinct operation modes of the moving platform. Further, Kong et al. synthesized reconfigurable parallel manipulators (RPMs) with multiple operation modes using the screw-based method [11, 12]. Gogu also investigated the geometric constraint singularity induced transitory phase of bifurcated platform motion in parallel manipulator and the mobility change [13]. Using the displacement group-based method, Li et al. presented a class of RPMs with bifurcation of Schoenflies motion [14]. Apart from the work on constructing reconfigurable parallel manipulators using traditional kinematic pairs, reconfigurable and lockable kinematic joints were invented for the purpose of developing reconfigurable parallel mechanisms. Gan et al. developed the reconfigurable hook (rT) joint for construction of metamorphic parallel mechanisms [15]. Zhang et al. presented the variable-Axis(vA) joint and integrated the three-phase joint in designs of a family of metamorphic parallel mechanisms [16]. Carbonari et al. designed a class of reconfigurable parallel manipulator by introducing a special lockable universal joint [17,18]. By integrating reconfigurable closed-loop subchains in the kinematic limbs of parallel mechanisms, novel reconfigurable parallel mechanism with hybrid limbs [19, 20] have been designed and synthesized in terms of screw theory [21, 22].

These work led to various structure design of reconfiguable parallel mechanisms and revealed multi-function characteristics of such mechanical systems. However, corresponding actuation methods and approaches for reconfiguration are yet comprehensively investigated. In other words, the way for switching the motion branches by passing a constraint singularity induced transitory position is still an open problem.

This paper presents a new reconfigurable parallel mechanism with Bennett plano-spherical linkages and uses inflatable bending actuators for switching motion branches. In the following sections, we first introduce the type-III Bennett plano-spherical linkages, which is a kinematic equivalent of a kirigami model and reveal the distinct motion branches of the linkage. Section III presents a reconfigurable parallel manipulator with hybrid kinematic limb and reveals motion characteristics of the parallel manipulator in different motion branches. Section IV addresses the kinematic model of the paralel manipulator. Section V details the proposed method for reconfiguring motion branches by using redundant inflatable bending actuators, and the paper is then concluded in Section V.

2 A Kirigami Model and Its Kinematic Equivalent

2.1 Crease Pattern for the Kirigami Model

The crease pattern for a kirigami model is shown in Fig. 1 where the solid lines AA$'$ and F$'$G$'$ are the creases for cutting while the dashed lines $R_j (j = 1, ..., 7)$ are the pre-grooved creases for folding. The creases R_1, R_4 and R_7 of the 2D crease pattern are colinear and parallel to the creases R_2 and R_6. The angle between creases R_3 and R_4 equals to that between R_4 and R_5. The angles are denoted by γ and equal to $\pi/4$. This implies that the crease pattern of the kirigami model is symmetric with respect to the line *BC* which is aligned with creases R_1 and R_4.

2.1.1 The Equivalent 6R Linkage.

For any thin sheet materials such as paper cardboard and smart composites with pre-grooved crease pattern shown in Fig. 1, it can be folded into different configurations including the typical one illustrated in Fig. 2(a). It shows that creases move away from the 2D plane and the degree-4 fold with vertex *C* is partially-folded. The creases R_1, R_4 and R_7 are coplanar with R_1 and R_7 parallel to each other. Based on the principle of artimimetics [23], a kinematic equivalent can be extracted from the kirigami model by taking creases as revolute joints and panels as links. Since the crease R_7, which is parallel to R_1, R_2 and R_6, corresponds rotating axis always passes point C, the kinematic equivalent can be simplified as an overconstrained 6R linkage by considering the crease R_7 as a virtual joint.

A kinematic model and of the 6R linkage is illustrated in Fig. 2(b). The vectors pointing in the direction of joint axes of joints R_i $(i = 1, 2, ..., 6)$ are denoted by $\mathbf{s}_i$. The axes of revolute joints R_1, R_2 and R_6 are parallel whilst the axes of joints R_3, R_4 and R_5 intersect at common point *C*. The 6R linkage is symmetric with respect to the plane Π_1 determined by axes of joints R_1 and R_4. The angle between axes of joints R_3 and R_4 and that between R_4 and R_5 are $\pi/4$. It implies that the symmetric 6R linkage is a type-III reconfigurable Bennett plano-spherical linkage [24].

The axes of joints $R_2(\mathbf{s}_2)$ and $R_3(\mathbf{s}_3)$ have a common point *F* and axes of joints $R_5(\mathbf{s}_5)$ and $R_6(\mathbf{s}_6)$ have common point *G*. In this general configuration, axes of joints $R_1(\mathbf{s}_1)$ and $R_4(\mathbf{s}_4)$ intersect at an instantaneous common point *E*. Given the plane-symmetric property of the 6R linkage, the projection of points *F* and *G* on the axis of joint R_1 are coincide, which is denoted by *O*. The distances measured from axes of joints R_1 and R_4 to points *F* and *G* are equal and denoted by *l*.

2.2 Motion branch variation of the Bennett plano-spherical linkage

The local coordinate frame $O-xyz$ with the origin attached at point *O* is set up for the 6R linkage. The *z*-axis is collinear with the axis of joint R_1, *x*-axis is located in the symmetric plane and *y*-axis is set following the right-handed rule. Thus

the linkage is symmetric with respect to the *xoz* plane of the reference frame. The position vectors of points C, E, F and G expressed in the local frame $O-xyz$ are given by

$$\begin{cases} \mathbf{r}_c = [2l\cos\theta \quad 0 \quad l]^{\mathrm{T}} \\ \mathbf{r}_e = [0 \quad 0 \quad l\cos^2\theta]^{\mathrm{T}} \\ \mathbf{r}_f = [l\cos\theta \quad -l\sin\theta \quad 0]^{\mathrm{T}} \\ \mathbf{r}_g = [l\cos\theta \quad l\sin\theta \quad 0]^{\mathrm{T}} \end{cases} \tag{1}$$

in which θ is the angle measured from x-axis to line OG. With the position vectors expressed in Eq. (1), the vectors $s_i (i = 1,2,...,6)$ in the direction of joint axes can be derived as

$$\begin{cases} \mathbf{s}_1 = [0 \quad 0 \quad 1]^{\mathrm{T}} \\ \mathbf{s}_2 = [0 \quad 0 \quad 1]^{\mathrm{T}} \\ \mathbf{s}_3 = [l\cos\theta \quad l\sin\theta \quad l]^{\mathrm{T}} \\ \mathbf{s}_4 = [2l\cos\theta \quad 0 \quad l\sin^2\theta]^{\mathrm{T}} \\ \mathbf{s}_5 = [l\cos\theta \quad -l\sin\theta \quad l]^{\mathrm{T}} \\ \mathbf{s}_6 = [0 \quad 0 \quad 1]^{\mathrm{T}} \end{cases} \tag{2}$$

Hence, motion screws, $\mathbf{S}_i = [\mathbf{s}, \mathbf{r}\times\mathbf{s}]^{\mathrm{T}}$, of the overconstrained 6R linkage in Fig. 2(b) expressed in the reference frame $O-xyz$ are

$$\begin{cases} \mathbf{S}_1 = [0 \quad 0 \quad 1 \quad 0 \quad 0 \quad 0]^{\mathrm{T}} \\ \mathbf{S}_2 = [0 \quad 0 \quad 1 \quad -l\sin\theta \quad -l\cos\theta \quad 0]^{\mathrm{T}} \\ \mathbf{S}_3 = [l\cos\theta \quad l\sin\theta \quad l \quad -l^2\sin\theta \quad -l^2\cos\theta \quad 2l^2\sin\theta\cos\theta]^{\mathrm{T}} \\ \mathbf{S}_4 = [2l\cos\theta \quad 0 \quad l\sin^2\theta \quad 0 \quad 2l^2\cos^3\theta \quad 0]^{\mathrm{T}} \\ \mathbf{S}_5 = [l\cos\theta \quad -l\sin\theta \quad l \quad -l^2\sin\theta \quad -l^2\cos\theta \quad -2l^2\sin\theta\cos\theta]^{\mathrm{T}} \\ \mathbf{S}_6 = [0 \quad 0 \quad 1 \quad l\sin\theta \quad -l\cos\theta \quad 0]^{\mathrm{T}} \end{cases} \tag{3}$$

By passing the transitory position, which is corresponding to the planar configuration of the Kirigami in Fig 1, the overconstrained 6R linkage reconfigures to the spherical 4R configuration in Fig. 3(a), the revolute joints R_2 and R_6 are geometrically constrained. Axes of all active joints R_1, R_3, R_4 and R_5 intersect at common point C which is now a fixed point on the axis of joint R_1. In this configuration, motion screws of this spherical 4R motion branch are

$$\begin{cases} \mathbf{S}_1 = [0 \quad 0 \quad 1 \quad 0 \quad 0 \quad 0]^{\mathrm{T}} \\ \mathbf{S}_3 = [-l\cos\theta \quad l\sin\theta \quad l \quad -l^2\sin\theta \quad -l^2\cos\theta \quad 0]^{\mathrm{T}} \\ \mathbf{S}_4 = [-2l\cos\theta \quad 0 \quad l\sin^2\theta \quad 0 \quad -2l^2\cos\theta \quad 0]^{\mathrm{T}} \\ \mathbf{S}_5 = [l\cos\theta \quad l\sin\theta \quad l \quad -l^2\sin\theta \quad l^2\cos\theta \quad 0]^{\mathrm{T}} \end{cases} \tag{4}$$

The overconstrained 6R linkage is also able to reconfigure to a planar parallelogram 4R linkage in Fig. 3(b) where the revolute joints R_3 and R_5 are geometrically constrained. In this configuration, axes of all four active joints R_1, R_2, R_4 and R_6 are parallel and motion screws expressed in the local frame change to

$$\begin{cases} \mathbf{S}_1 = [0 \quad 0 \quad 1 \quad 0 \quad 0 \quad 0]^{\mathrm{T}} \\ \mathbf{S}_2 = [0 \quad 0 \quad 1 \quad -l\sin\theta \quad -l\cos\theta \quad 0]^{\mathrm{T}} \\ \mathbf{S}_4 = [0 \quad 0 \quad 1 \quad 0 \quad -2l\cos\theta \quad 0]^{\mathrm{T}} \\ \mathbf{S}_6 = [0 \quad 0 \quad 1 \quad l\sin\theta \quad -l\cos\theta \quad 0]^{\mathrm{T}} \end{cases} \tag{5}$$

3 Motion Branch Variation of the Reconfigurable Parallel Manipulator

3.1 The parallel manipulator with reconfigurable Bennett Plano-Spherical Subchain

The parallel manipulator shown in Fig 4 has a triangular base and a platform connected by three identical hybrid kinematic limbs. Each limb consists of a revolute joint whose axis colinear with axis of R_{i1}, a Bennett plano-spherical linkage, and three revolute joints in consequence. Geometric centres of the equilateral triangular base $\triangle B_1B_2B_3$ and the platform $\triangle P_1P_2P_3$ are labeled O_b and O_p, respectively. As illustrated in Fig. 4, axes of the three parallel revolute joints of the Bennett plano-spherical subchain are perpendicular to the base and the axis of joint R_{i1} passes vertex B_i, where $i = 1,2,3$ denotes sequential number of the limbs. This forms a compound kinematic joint at B_i. The axis of joint R_{i7} is collinear with the axis of joint R_{i4} and the two joints form another compound kinematic joint in the limb. The axis of joint R_{i8} is perpendicular to the axis of R_{i7} without intersection. The last revolute joint R_{i9} connects the limb to the platform and have a common point with axis of joint R_{i8}. Further, the axes of joints R_{i8} and R_{i9} of all three limbs share common point P. This common point and the other three vertices P_i of the platform form a virtual tetrahedron. The unit vector representing rotational axis of revolute joints R_{ij} in the i-th limb is denoted $s_{ik}(i = 1,2,3;k = 0,1,...,9)$. In the configuration shown in Fig. 4, vectors $\mathbf{s}_{i1}$, $\mathbf{s}_{i2}$, $\mathbf{s}_{i3}$ are parallel. A global coordinate frame $O_b - XYZ$ with the origin attached at point O_b is set up for the parallel manipulator. The Z-axis is perpendicular to the base and pointing upward, X-axis is located in the base plane and passes point B_1 and Y-axis is set following the right-handed rule.

3.2 The transitory configuration of the reconfigurable parallel manipulator

As revealed in the Section above, the type-III Bennett plano-spherical linkage is able to reconfigure its configuration between three distinct motion branches, i.e. overconstrained 6R linkage (Fig. 2(b)), spherical 4R (Fig. 3(a)) and planar 4R (Fig. 3(b)) linkages. As a result, each hybrid limb of the parallel manipulator in Fig. 4 is able to change its configuration due to the reconfigurability of the type-III Bennett plano-spherical linkage. For this closed-loop subchain, the constraint singularity occurs when joint R_{i4} is colinear with R_{i1}. It implies that axis of joint R_{i7} is perpendicular to the XOY plane in the transitory configuration. When all Bennett plano-spherical linkages in the three limbs are at their transitory configuration, the parallel manipulator is at its transitory configuration whose top view is illustrated in Fig. 5.

As aforementioned, axis of joint R_{i8} is perpendicular to the plane defined by axis of joints R_{i7} and C_iD_i and passes the common point P. In this transitory configuration, axes of joints R_{i8} in all three limbs are parallel to the XOY plane and Z-axis passes the common point P. Assuming l_{cd} is length of the common normal of the two non-intersecting axes of joints R_{i7} and R_{i8} and the distance between points P and D_i is a design parameter denoted by l_{dp}. Based on the geometrical condition, l_{cd} and l_{dp} must satisfy the following constraints so that the transitory configuration exists, that is

$$l_{cd}^2 + l_{dp}^2 = a^2 \tag{6}$$

where a is the distance between points B_i and O_b.

3.3 The 6-DOF motion branch

When the three hybrid limbs of the parallel manipulator are in the same motion branch with the closed-loop subchain working as the overconstrained 6R linkage, all joints in each limb are active and the parallel manipulator is in the motion branch illustrated in Fig. 4. In this motion branch, the closed-loop subchain is equivalent to a serial kinematic chain composed of $R_{i1}R_{i2}R_{i3}R_{i4}$ with axis of joint R_{i4} restricted in the symmetric plane of the 6R linkage. As axis of joint R_{i7} is colinear with that of R_{i4}, the passive compound joint is simplified as one revolute joint and the hybrid limb is equivalent to a 6R serial kinematic chain denoted by $R_{i1}R_{i2}(R_{i3}R_{i4})(R_{i8}R_{i9})$, where R_{ij} in a bracket representing joints intersecting at a common point. The motion screws $\mathbf{S}_{ij}(j = 1,2,3,4)$ in Eq.(3) are independent and all six revolute joints are not meeting one common line in this non-singular configuration. It implies that motion-screw system of the equivalent serial kinematic limb provides no constraints. Hence, moving platform of the parallel manipulator in this motion branch (Fig. 4) has 6 DOFs.

3.4 The 3-DOF spherical motion branch

When the three hybrid limbs of the parallel manipulator are in the same configuration where all closed-loop subchains change to spherical 4R linkages (Fig. 3(a)), the parallel manipulator reconfigures to the motion branch illustrated in Fig. 6.

In this motion branch, axis of joint R_{i4} is rotating along a virtual axis passing common point C_i. The spherical 4R closed-loop subchain together with the joint R_{i7}, whose axis is colinear with axis of R_{i4}, equivalent to a spherical joint with spherical center C_i. Hence, the hybrid limb is equivalent to a 5R serial kinematic chain denoted by $(R_{v1}R_{v2}R_{v3})(R_{i8}R_{i9})$, where '$v$' in subscripts denotes the equivalent revolute joint of the virtual spherical joint. In this case, a new local frame $O_i - x_iy_iz_i$ is set with the origin at spherical center C_i, x_i-axis parallel to the axis of joint R_{i8}, y_i-axis the common normal of z_i-axis and axis of R_{i8}. The motion-screw system of the equivalent serial kinematic chain expressed in the frame $O_i - x_iy_iz_i$

is

$$\begin{cases} \mathbf{S}_{v1} = [1 \quad 0 \quad 0 \quad 0 \quad 0 \quad 0]^{\mathrm{T}} \\ \mathbf{S}_{v2} = [0 \quad 1 \quad 0 \quad 0 \quad 0 \quad 0]^{\mathrm{T}} \\ \mathbf{S}_{v3} = [0 \quad 0 \quad 1 \quad 0 \quad 0 \quad 0]^{\mathrm{T}} \\ \mathbf{S}_{i8} = [1 \quad 0 \quad 0 \quad 0 \quad 0 \quad -b]^{\mathrm{T}} \\ \mathbf{S}_{i9} = [l_{i9} \quad m_{i9} \quad n_{i9} \quad bn_{i9} \quad -an_{i9} \quad am_{i9} - bl_{i9}]^{\mathrm{T}} \end{cases} \tag{7}$$

where $\mathbf{s}_{i9} = [l_{i9}\ m_{i9}\ n_{i9}]^{\mathrm{T}}$ represents the direction of axis of joint R_{i9} and $[a\ b\ 0]^{\mathrm{T}}$ is the position vector of the common point P.

With motion screws in Eq.(7), the constraint screws reciprocal to the motion screws of the equivalent serial kinematic chain are calculated as

$$\mathbf{S}_{11}^{\mathrm{r}} = [a \quad b \quad 0 \quad 0 \quad 0 \quad 0]^{\mathrm{T}} \tag{8}$$

The above screw represents a constraint force colinear with line PC_i.

The three limbs thus exert three constraint forces to the platform and all three forces passing common point P. These constraint forces restrict all transnational motions of the platform. As a result, the platform implements 3-DOF spherical motion with the motion centre at common point P. This configuration equivalents to conventional 3-DOF spherical parallel mechanisms presented in [25–27].

3.5 The 5-DOF mixed motion branch

When the closed-loop subchain in each limb changes to the planar 4R linkage in Fig. 3 (b), the parallel manipulator reconfigures to its third motion branch in Fig. 7.

With a planar 4R parallelogram linkage subchain, the hybrid limb is equivalent to a 5R serial kinematic chain denoted by $\mathrm{R}_{i1}\mathrm{R}_{i2}\mathrm{R}_{i7}(\mathrm{R}_{i8}\mathrm{R}_{i9})$. Since joint R_{i7} is colinear with the z_i-axis, axis of joint R_{i8} parallel to $x_io_iy_i$ plane. The motion screws of the equivalent serial kinematic chain in the reference frame $O_i - x_iy_iz_i$ are given by

$$\begin{cases} \mathbf{S}_{i1} = [0 \quad 0 \quad 1 \quad 0 \quad 0 \quad 0]^{\mathrm{T}} \\ \mathbf{S}_{i2} = [0 \quad 0 \quad 1 \quad -l\sin\theta \quad -l\cos\theta \quad 0]^{\mathrm{T}} \\ \mathbf{S}_{i7} = [0 \quad 0 \quad 1 \quad 0 \quad -2l\cos\theta \quad 0]^{\mathrm{T}} \\ \mathbf{S}_{i8} = [\cos\beta \quad \sin\beta \quad 0 \quad -e\sin\beta \quad e\cos\beta \quad c\sin\beta - d\cos\beta]^{\mathrm{T}} \\ \mathbf{S}_{i9} = [l_{i9} \quad m_{i9} \quad n_{i9} \quad dn_{i9} - em_{i9} \quad el_{i9} - cn_{i9} \quad cm_{i9} - dl_{i9}]^{\mathrm{T}} \end{cases} \tag{9}$$

where $\mathbf{s}_{i8} = [\cos\beta\ \ \sin\beta\ \ 0]^{\mathrm{T}}$ and $\mathbf{s}_{i9} = [l_{i9}\ m_{i9}\ n_{i9}]^{\mathrm{T}}$ represent vectors pointing in the axis direction of joints R_{i8} and R_{i9}, respectively, and $[c\ d\ e]^{\mathrm{T}}$ is the position vector of the common point P.

The constraint screws reciprocal to the above motion screws of the equivalent serial kinematic chain are calculated as

$$\mathbf{S}_{11}^{\mathrm{r}} = [0 \quad 0 \quad 1 \quad d \quad -c \quad 0]^{\mathrm{T}} \tag{10}$$

This screw represents a constraint force which passes the common point P and parallel to z_i-axis.

Considering geometry of the parallel manipulator in Fig.7, all three limbs provide a common constraint force passing point P and parallel to Z-axis of global reference frame $O-XYZ$. Under such a constraint force, only the translation along Z-axis is restricted. The moving platform of the parallel manipulator has 5 DoFs and implements 2 DoFs translation and 3 DoFs rotation with spherical center P, which moves in a plane parallel to XO_bY plane. This configuration equivalents to conventional 5-DOF spherical parallel mechanisms identified in [28, 29].

4 Kinematics Analysis of the Reconfigurable Parallel Manipulator

The above section proves that the reconfigurable parallel manipulator has three distinct mobility configurations induced by the configuration variation of the type-III reconfigurable Bennett plano-spherical linkage. Here we establish a unified

kinematics model and reveals the parameters that characterize internal connections and switch between different configurations.

As illustrated in Fig. 4, the revolute joints R_{i1} connecting limbs to the base are symmetrically located with joint axes pass vertices B_1, B_2 and B_3 respectively of the equilateral triangle whose circumradius is r. It is worth to point out that each common point C_i traces a straight line in the plane defined by axes R_{i1} and R_{i4} and parallel to the base plane defined by B_1, B_2 and B_3. With such geometrical characteristics of the parallel manipulator, a kinematic diagram is illustrated in Fig. 8 aimed at kinematics analysis.

In a general configuration, the reconfigurable parallel manipulator is in its 6-DOF configuration where the platform implements 3 DOFs rotations and 3 DOFs translation. Each limb has two input joints, including the first revolute joint R_{i0} connecting the limb to the base and the consecutive revolute joint R_{i1} that defines the configuration of the Bennett plano-spherical linkage. The rotational input variables in limb i are denoted as θ_i and φ_i.

Position of moving platform can be expressed using the vector $\mathbf{O_p} = [x, y, z]^{\mathrm{T}}$ of the origin O_p. To express the orientation of the moving platform with respect to the global coordinate frame, the $Z-Y-X$ Euler angles are used here. The rotation matrix is expressed as

$$\begin{aligned}\mathbf{R}_p &= \mathbf{R}_{xyz}(\gamma, \beta, \alpha) \\ &= \begin{bmatrix} c\alpha c\beta & c\alpha s\beta s\gamma - s\alpha c\gamma & c\alpha s\beta c\gamma + s\alpha s\gamma \\ s\alpha c\beta & s\alpha s\beta s\gamma + c\alpha c\gamma & s\alpha s\beta c\gamma - c\alpha s\gamma \\ -s\beta & c\beta s\gamma & c\beta c\gamma \end{bmatrix}\end{aligned} \tag{11}$$

where the subscript p denotes the local reference frame of platform, $c*$ and $s*$ denote $\cos(*)$ and $\sin(*)$, respectively.

Position vectors of vertices $B_i (i = 1, 2, 3)$ in the global coordinate frame can be expressed as

$$\begin{aligned}\mathbf{B}_1 &= [a, 0, 0]^{\mathrm{T}} \\ \mathbf{B}_2 &= \left[-\frac{a}{2}, \frac{\sqrt{3}a}{2}, 0\right]^{\mathrm{T}} \\ \mathbf{B}_3 &= \left[-\frac{a}{2}, -\frac{\sqrt{3}a}{2}, 0\right]^{\mathrm{T}}\end{aligned} \tag{12}$$

Since the common point C_i traces a straight line parallel to the base plane, position vector of A, the projection of point C_i on axis of joint R_{i1}, is given by

$$\begin{aligned}\mathbf{A}_1 &= [a, 0, h]^{\mathrm{T}} \\ \mathbf{A}_2 &= \left[-\frac{a}{2}, \frac{\sqrt{3}a}{2}, h\right]^{\mathrm{T}} \\ \mathbf{A}_3 &= \left[-\frac{a}{2}, -\frac{\sqrt{3}a}{2}, h\right]^{\mathrm{T}}\end{aligned} \tag{13}$$

where h is a constant design parameter denoting the distance between points B_i and A_i.

According to [30], the position vector of points C_i in the local frame $B_i - xyz$ can be expressed as

$${}^{bi}\mathbf{C}_i = [d_i \cos(\theta_i + \frac{\varphi_i}{2}), d_i \sin(\theta_i + \frac{\varphi_i}{2}), h]^{\mathrm{T}} \tag{14}$$

where $d_i = 2r\cos\frac{\varphi_i}{2}$ is the distance between points C_i and A_i and determined by the rotational input φ_i of joint R_{i1} and the link length r

Hence, the position vector of points C_i in the global frame $O_b - XYZ$ can then be derived as

$$\mathbf{C}_i = \mathbf{R}(\psi_i) \cdot {}^{bi}\mathbf{C}_i + \mathbf{B}_i \tag{15}$$

where $\mathbf{R}(\psi_i)$ is the rotational matrix about Z-axis with rotational angle $\psi_1 = 0, \psi_2 = 2\pi/3$, and $\psi_3 = -2\pi/3$.

With the specific geometry of the moving platform, the common point P is on the w-axis and its position vectors in the local coordinate frame $O_p - uvw$ can be expressed as

$$^{p}\mathbf{P} = [0, 0, z_p]^{\mathrm{T}} \tag{16}$$

where the left superscript p denotes the reference frame. Position vectors of points P expressed in the global coordinate frame can be given by

$$\mathbf{P} = \mathbf{R}_p \cdot {}^{p}\mathbf{P} + \mathbf{O_p} \tag{17}$$

Given the above position vectors, a closed-loop constraint equation for the ith limb can be obtained as

$$|\mathbf{C}_i\mathbf{P}| = d_{cip} \tag{18}$$

where $\mathbf{C}_i\mathbf{P} = \mathbf{C}_i - \mathbf{P}$, and d_{cip} is a constant design parameter defining distance between points C_i and P.

Substituting Eqs. 15 and 17 into Eq. 18 yields

$$\begin{aligned}((h-z-z_pc\beta c\gamma)^2+(a-x+r(c\theta_1+c(\theta_1+\varphi_1))-z_p(c\alpha c\gamma s\beta+s\alpha s\gamma))^2+(y+z_pc\gamma s\alpha s\beta-z_pc\alpha s\gamma \\ -r(s\theta_1+s(\theta_1+\varphi_1)))^2)^{1/2}=d_{c1p}\end{aligned} \tag{19}$$

$$\begin{aligned}\frac{1}{2}((4(h-z-z_pc\beta c\gamma)^2+(\sqrt{3}a-2y+\sqrt{3}rc\theta_2+\sqrt{3}rc(\theta_2+\varphi_2)-2z_pc\gamma s\alpha s\beta+2z_pc\alpha s\gamma-r(s\theta_2 \\ +s(\theta_2+\varphi_2)))^2+(a+2x+2z_p(c\alpha c\gamma s\beta+s\alpha s\gamma)+r(c\theta_2+c(\theta_2+\varphi_2)+\sqrt{3}(s\theta_2+s(\theta_2+\varphi_2))))^2)^{1/2}=d_{c2p}\end{aligned} \tag{20}$$

$$\begin{aligned}\frac{1}{2}((4((h-z-z_pc\beta c\gamma)^2+(\frac{\sqrt{3}}{2}a+y+\frac{1}{2}r(\sqrt{3}c\theta_3+\sqrt{3}c(\theta_3+\varphi_3)+s\theta_3+s(\theta_3+\varphi_3))+z_pc\gamma s\alpha s\beta \\ -z_pc\alpha s\gamma)^2)+(a+2x+2z_p(c\alpha c\gamma s\beta+s\alpha s\gamma)+r(c\theta_3+c(\theta_3+\varphi_3)-\sqrt{3}(s\theta_3+s(\theta_3+\varphi_3))))^2)^{1/2}=d_{c3p}\end{aligned} \tag{21}$$

According to the geometrical conditions of the Bennett plano-spherical linkage [30], the vector $\mathbf{n}_{i4}$ pointing in the direction of joint axes of R_{i4} and R_{i7} in the local frame $B_i - xyz$ can be expressed as

$$^{bi}\mathbf{n}_{i4} = [d_i\cos(\theta_i+\frac{\varphi_i}{2}), d_i\sin(\theta_i+\frac{\varphi_i}{2}), r]^{\mathrm{T}} \tag{22}$$

The directional vector $\mathbf{n}_{i4}$ in the global frame is then derived as

$$\mathbf{n}_{i4} = \mathbf{R}(\psi_i) \cdot {}^{bi}\mathbf{n}_{i4} \tag{23}$$

As aforementioned, the colinear axes of joint R_{i4} and R_{i7} are perpendicular to the plane defined by axis of joint R_{i8} and C_iP. It implies that vectors $\mathbf{n}_{i4}$ is perpendicular to vector $\mathbf{C}_i\mathbf{P}$, meaning $\mathbf{n}_{i4} \cdot \mathbf{C}_i\mathbf{P} = 0$. This leads to three constraint equations

$$\begin{aligned}r(h+2r-z-z_pc\beta c\gamma+2rc\varphi_1+(a-x)(c\theta_1+c(\theta_1+\varphi_1))-2z_pc\frac{\varphi_1}{2}(c\gamma c(\alpha-\theta_1-\frac{\varphi_1}{2})s\beta \\ +s\gamma s(\alpha-\theta_1-\frac{\varphi_1}{2}))-y(s\theta_1+s(\theta_1+\varphi_1)))=0\end{aligned} \tag{24}$$

$$\frac{1}{2}r(2h+4r-2z-2z_pc\beta c\gamma+4rc\varphi_2+(2a+x-\sqrt{3}y)(c\theta_2+c(\theta_2+\varphi_2))+2z_pc\frac{\varphi_2}{2}(s\gamma(\sqrt{3}c(\alpha-\theta_2-\frac{\varphi_2}{2}) \\ +s(\alpha-\theta_2-\frac{\varphi_2}{2}))+c\gamma s\beta(c(\alpha-\theta_2-\frac{\varphi_2}{2})-\sqrt{3}s(\alpha-\theta_2-\frac{\varphi_2}{2})))+(\sqrt{3}x+y)(s\theta_2+s(\theta_2+\varphi_2)))=0 \tag{25}$$

$$\frac{1}{2}r(2h+4r-2z-2z_pc\beta c\gamma+4rc\varphi_3+(2a+x+\sqrt{3}y)(c\theta_3+c(\theta_3+\varphi_3))+2z_pc\frac{\varphi_3}{2}(s\gamma(-\sqrt{3}c(\alpha-\theta_3-\frac{\varphi_3}{2}) \\ +s(\alpha-\theta_3-\frac{\varphi_3}{2}))+c\gamma s\beta(c(\alpha-\theta_3-\frac{\varphi_3}{2})+\sqrt{3}s(\alpha-\theta_3-\frac{\varphi_3}{2})))-(\sqrt{3}x-y)(s\theta_3+s(\theta_3+\varphi_3)))=0 \tag{26}$$

The analysis above reveals that the reconfigurable parallel manipulator is fully actuated when it is in the configuration with 6 DOFs in Fig. 4, and there are six input variables, i.e. $\theta_1,\theta_2,\theta_3,\varphi_1,\varphi_2,\varphi_3$, and six independent output parameters $x,y,z,\alpha,\beta,\gamma$. The mapping between input variables and output parameters are established in Eqs. 19- 21 and 24- 26.

When the parallel manipulator reconfigures to the motion branch with 3 DOFs spherical motion in Fig. 6, the points C_i are located on the axis of joint R_{i1} due to geometrical constraints. It implies that points C_i and A_i are coincide and $d_i=0$. Hence, the position vector of point C_i expressed in the local frame B_i-xyz becomes ${}^{bi}\mathbf{C}_i=[0,0,h]^{\mathrm{T}}$. In this configuration, the parallel manipulator is redundantly actuated with all six input variables.

When the parallel manipulator reconfigures to the motion branch with 5 DOFs mixed motion in Fig. 7, the collinear axes of joints R_{i4} and R_{i7} are parallel to that of R_{i1}. It implies that vectors $\mathbf{n}_{i4}$ are parallel to the Z-axis and the Eq. 22 becomes ${}^{bi}\mathbf{n}_{i4}=[0,0,h]^{\mathrm{T}}$. Hence, the constraint equations in Eqs. 24-26 changes to

$$h(h-z-z_pc\beta c\gamma)+a(a-x+r(c\theta_1+c(\theta_1+\varphi_1)-z_p(c\alpha c\gamma s\beta+s\alpha s\gamma))=0 \tag{27}$$

$$\frac{1}{2}(a(2a+x-\sqrt{3}y)+2h(h-z)-2hz_pc\beta c\gamma+a(2r(c\theta_2+c(\theta_2+\varphi_2))+z_ps\beta c\gamma(c\alpha-\sqrt{3}s\alpha) \\ +z_p(\sqrt{3}c\alpha+s\alpha)s\gamma))=0 \tag{28}$$

$$\frac{1}{2}(a(2a+x+\sqrt{3}y)+2h(h-z)-2hz_pc\beta c\gamma+a(2r(c\theta_3+c(\theta_3+\varphi_3))+z_ps\beta c\gamma(c\alpha+\sqrt{3}s\alpha) \\ +z_p(-\sqrt{3}c\alpha+s\alpha)s\gamma))=0 \tag{29}$$

Further, the point P is restricted in a plane parallel to the base plane. It gives an additional constraints that $h-z-z_pc\beta c\gamma=0$. In this configuration, the parallel manipulator is redundantly actuated with all six input variables.

5 A Novel Inflatable Bending Actuator for Reconfiguring a Foldable Bennett Plano-Spherical Linkage

Pneumatic actuation is used in many industrial applications [31] and has been extensively employed in the soft robotics [32]. This section introduces the design and fabrication of origami-folding [33, 34] inspired inflatable bending actuator which can be integrated with a type-III foldable Bennett plano-spherical linkage for motion branch reconfiguration.

5.1 Design of a novel inflatable bending actuator

Recent research has shown that a airbag made of quasi-inextensible materials turns to a balloon-like structure once inflated [32]. In most of the airbag actuator designs, the softness of thin film materials allows deformation of the lateral seams in the process of inflation. Normally, both layers of the airbag are thin film materials and the deformation is not uniform. Aimed at creating a bending hinge and actively controlling the rotating direction of passive joints at the transitory configuration of a reconfigurable mechanism, here a new type of airbag actuator is proposed by combining a foldable origami base and layers of thin quasi-inextensible material.

The rigid foldable origami base is termed as rectangular tile with a line-symmetric crease pattern illustrated in Fig.9, consisting of two degree-4 single-vertex folds. The dashed lines indicate the location of a valley folds and the dash-dot-dot lines indicate the location of a mountain folds. The strip between the edges and offset dashed lines is the area created for sealing the airbag. When the airbag is not inflated (Fig.9 (a)), the thin film tightly attaches to the origami panels and passively

rotating around the axis O_1O_2 since the thin film material will not significantly increase the thickness of the origami base. Once inflated, the airbag deforms and the seam between c_1 and c_3 and that between c_4 and c_6 will continue to curve. As the thin film deforms, creases c_2 and c_5 fold towards each other and the two panels between c_1 and c_6 and that between c_4 and c_5 are actively rotating around the joint axis O_1O_2 until the volume in the airbag is maximized. As such, the origami based airbag always bends towards the thin film side.

5.2 Fabrication of the multi-layered inflatable bending actuator

In this work, a two-layered airbag is produced as a prototype to verify the concept of the proposed pneumatic inflatable bending actuator. The origami base is fabricated by folding a thin sheet paper card (300 microns) with preprinted crease pattern. A type of airtight self adhesive polyurethane (TPU) fabric sheet of 100 microns is selected as the thin film material of the airbag. To create an airbag actuator, two layers of TPU fabric are used. The first layer of TPU fabric with same size of the origami base is firmly stuck to one side of the base with edges aligned. The second piece of TPU fabric with double size of the seam region only sticks to the seam regions along the edge of the origami base. The original non-sticking film attached inside the TPU fabric separates the TPU fabric and the origami base thus creating an airbag. A silicone tube (inside diameter (ID) = 1 mm) is firmly affixed between the two layers of TPU fabric and the connection between the tube and the airbag is further sealed with additional fabric to avoid air leaking. A prototype of the bending actuator is shown in Fig. 10, where the actively inflated bending (Fig. 10 (a) and (b)) and passive bending (Fig. 10 (c)) are demonstrated.

5.3 Integration of the bending actuator with a Bennett plano-spherical linkage and parallel manipulator

With advanced additive manufacturing and 3D printing technologies, foldable origami/kirigami model [35] can be 3D printed and then attached to layers of adhesive thin film materials to make a kinematic structure [36]. Here we select TPU filament as the model material given its flexible and durable properties. A thin TPU layer printed between the panels and printing bed is adopted as flexible hings of origami/kirigami structures. Using this fabrication approach and TPU material, a foldable Bennett plano-spherical linkage corresponding to the kirigami model in Fig. 1 is first printed. The inflatable bending actuator (Fig. 10) is then integrated with the printed Bennett plano-spherical mechanism by aligning the axis O_1O_2 of the actuator with the axis of joint R_4 of the mechanism (Fig. 11(a)).

As indicated in the kinematic analysis, the reconfigurable parallel manipulator has six input parameters and needs six rotary actuators in total. The pneumatic bending actuator integrated with the joint R_i4 is used as a redundant actuator to bend joint R_4 towards desired direction from the flat configuration (Fig. 11 (b)), which is also the transitory position of the 6R linkage, to one of the three motion branches. In order to move from the overconstrained 6R linkage and the parallel manipulator to other motion branches, the 6R linkage needs to first move to this transitory position. By passing the transitory position of the 6R linkage, the parallel manipulator is able to reconfigure to the 3-DOF spherical motion branch where the 6R linkage switches to its spherical 4R motion branch (Fig. 11 (c)) by inflating the bending actuator with a source of pressured air. After moving the 6R linkage out of the transitory position, the bending actuator is vacuumed to allow passive bending. Using the same redundant bending actuator, the parallel manipulator is also able to reconfigure to the 5-DOF motion branch where the 6R linkage changes to its planar 4R motion branch (Fig. 11 (d)).

6 Conclusions

This paper presented a type-III Bennett plano-spherical linkage which is a kinematic equivalent of a kirigami model and revealed the reconfigurability and three distinct motion branches of the linkage. A parallel manipulator is then designed by employing the Bennett plano-spherical linkage as closed-loop subchain of hybrid limbs. According to geometry and motion branch variation of the subchain, constraints of the hybrid limbs were derived by analysing equivalent serial kinematic limbs in terms of screw theory. It further revealed that the new parallel manipulator has three distinct motion branches. The motion platform of parallel manipulator has 6 DOFs full motion when the closed-loop subchains are 6R linkages. The moving platform performs 3 DoFs spherical motion when the closed-loop subchains all change to spherical 4R linkages. By passing the transitory position, the parallel manipulator is also able to reconfigure to a motion branch with 3 DoFs rotation and 2 DoFs translation. The mapping between joint inputs and platform outputs is revealed by the unified kinematics model for all three motion branches of the parallel manipulator. A new inflatable bending actuator is designed and fabricated by stacking three layers thin sheet materials including a rigid foldable rectangular tile origami base and two layers self-adhesive TPU fabric. Prototypes of the parallel manipulator and the foldable Bennett plano-spherical linkages with integrated inflatable bending actuator were fabricated. The preliminary prototypes prove that the proposed inflatable actuator is able to facilitate configuration change and switch between motion branches of reconfiguable mechanism with thin sheet panels. This work initiates a new trend for developing reconfigurable soft parallel manipulators.

The future work will focus on velocity analysis of the parallel manipulator and development of a complete prototype and inflatable actuator based actuation systems of the Bennett plano-spherical linkage and the reconfigurable parallel manipulator.

Acknowledgements

This work was partially supported by research awards from the Engineering and Physical Sciences Research Council (EPSRC) under grant agreements EP/R02572X/1 and National Centre for Nuclear Robotics (NCNR) Flexifund. Ketao Zhang is supported by the Royal Society Research Grant under grant agreement RGS\R1\211326.

References

[1] Merlet, J.-P., 2000. "Parallel robots: Open problems". In *Robotics research*. Springer, pp. 27–32.

[2] Wang, L., Wu, J., Wang, J., and You, Z., 2009. "An experimental study of a redundantly actuated parallel manipulator for a 5-dof hybrid machine tool". *IEEE/ASME Transactions on Mechatronics,* **14**(1), pp. 72–81.

[3] Jin, Y., Chanal, H., and Paccot, F., 2015. *Parallel Robots*. Springer London, pp. 2091–2127.

[4] Gan, D., Dai, J. S., Dias, J., and Seneviratne, L. D., 2016. "Variable motion/force transmissibility of a metamorphic parallel mechanism with reconfigurable 3t and 3r motion". *Journal of Mechanisms and Robotics,* **8**(5).

[5] Kang, X., and Dai, J. S., 2019. "Relevance and transferability for parallel mechanisms with reconfigurable platforms". *Journal of Mechanisms and Robotics,* **11**(3).

[6] Daniel Finistauri, A., et al., 2013. "Reconfiguration analysis of a fully reconfigurable parallel robot". *Journal of Mechanisms and Robotics,* **5**(4).

[7] Essomba, T., Hsu, Y., Sandoval Arevalo, J. S., Laribi, M. A., and Zeghloul, S., 2019. "Kinematic optimization of a reconfigurable spherical parallel mechanism for robotic-assisted craniotomy". *Journal of Mechanisms and Robotics,* **11**(6).

[8] Yang, H., Fang, H., Li, X., and Fang, Y., 2020. "Workspace augmentation for the large-scale spherical honeycombs perfusion using a novel 5dof reconfigurable manipulator". *Journal of Mechanisms and Robotics,* **12**(6).

[9] Zlatanov, D., Bonev, I. A., and Gosselin, C. M., 2002. "Constraint singularities as c-space singularities". In *Advances in robot kinematics*. Springer, pp. 183–192.

[10] Zlatanov, D., Bonev, I. A., and Gosselin, C. M., 2002. "Constraint singularities of parallel mechanisms". In Proceedings 2002 IEEE International Conference on Robotics and Automation (Cat. No. 02CH37292), Vol. 1, IEEE, pp. 496–502.

[11] Kong, X., Gosselin, C. M., and Richard, P.-L., 2006. "Type synthesis of parallel mechanisms with multiple operation modes". *Journal of Mechanical Design,* **129**(6), 06, pp. 595–601.

[12] Kong, X., and Yu, J., 2015. "Type synthesis of two-degrees-of-freedom 3-4r parallel mechanisms with both spherical translation mode and sphere-on-sphere rolling mode". *Journal of Mechanisms and Robotics,* **7**(4).

[13] Gogu, G., 2009. "Branching singularities in kinematotropic parallel mechanisms". In *Computational kinematics*. Springer, pp. 341–348.

[14] Li, Q., and Hervé, J. M., 2009. "Parallel mechanisms with bifurcation of schoenflies motion". *IEEE Transactions on Robotics,* **25**(1), pp. 158–164.

[15] Gan, D., Dai, J. S., and Liao, Q., 2010. "Constraint analysis on mobility change of a novel metamorphic parallel mechanism". *Mechanism and Machine Theory,* **45**(12), pp. 1864–1876.

[16] Zhang, K., Dai, J. S., and Fang, Y., 2013. "Geometric constraint and mobility variation of two 3svpsv metamorphic parallel mechanisms". *Journal of Mechanical Design,* **135**(1).

[17] Carbonari, L., Callegari, M., Palmieri, G., and Palpacelli, M.-C., 2014. "A new class of reconfigurable parallel kinematic machines". *Mechanism and Machine Theory,* **79**, pp. 173–183.

[18] Palpacelli, M.-C., Carbonari, L., Palmieri, G., and Callegari, M., 2014. "Analysis and design of a reconfigurable 3-dof parallel manipulator for multimodal tasks". *IEEE/Asme Transactions on Mechatronics,* **20**(4), pp. 1975–1985.

[19] Zhang, K., Dai, J. S., and Fang, Y., 2010. "Topology and constraint analysis of phase change in the metamorphic chain and its evolved mechanism". *Journal of Mechanical Design,* **132**(12), p. 121001.

[20] Zeng, Q., Fang, Y., and Ehmann, K. F., 2011. "Design of a novel 4-dof kinematotropic hybrid parallel manipulator". *Journal of Mechanical Design,* **133**(12).

[21] Dai, J. S., Huang, Z., and Lipkin, H., 2006. "Mobility of overconstrained parallel mechanisms". *Journal of Mechanical Design,* **128**(1), pp. 220–229.

[22] Zhao, J.-S., Feng, Z.-J., Zhou, K., and Dong, J.-X., 2005. "Analysis of the singularity of spatial parallel manipulator with terminal constraints". *Mechanism and Machine Theory,* **40**(3), pp. 275–284.

[23] Zhang, K., Fang, Y., Fang, H., and Dai, J. S., 2010. "Geometry and constraint analysis of the three-spherical kinematic chain based parallel mechanism". *Journal of Mechanisms and Robotics,* **2**(3).

[24] Chen, Y., 2003. "Design of structural mechanisms". PhD thesis, Oxford University, UK.

[25] Huang, Z., and Li, Q., 2002. "General methodology for type synthesis of symmetrical lower-mobility parallel manipulators and several novel manipulators". *The International Journal of Robotics Research,* **21**(2), pp. 131–145.

[26] Kong, X., and Gosselin, C. m. M., 2004. "Type synthesis of 3-dof spherical parallel manipulators based on screw theory". *J. Mech. Des.,* **126**(1), pp. 101–108.

[27] Hernandez, A., Ibarreche, J. I., Petuya, V., and Altuzarra, O., 2014. "Structural synthesis of 3-dof spatial fully parallel manipulators". *International Journal of Advanced Robotic Systems,* **11**(7), p. 101.

[28] Fang, Y., and Tsai, L.-W., 2002. "Structure synthesis of a class of 4-dof and 5-dof parallel manipulators with identical limb structures". *The international journal of Robotics Research,* **21**(9), pp. 799–810.

[29] Hu, B., 2019. "Terminal position and orientation coupling in lower mobility robots". *Journal of Mechanisms and Robotics,* **11**(3).

[30] Zhang, K., and Dai, J. S., 2015. "Screw-system-variation enabled reconfiguration of the bennett plano-spherical hybrid linkage and its evolved parallel mechanism". *Journal of Mechanical Design,* **137**(6).

[31] Mosadegh, B., Polygerinos, P., Keplinger, C., Wennstedt, S., Shepherd, R. F., Gupta, U., Shim, J., Bertoldi, K., Walsh, C. J., and Whitesides, G. M., 2014. "Pneumatic networks for soft robotics that actuate rapidly". *Advanced functional materials,* **24**(15), pp. 2163–2170.

[32] Ou, J., Skouras, M., Vlavianos, N., Heibeck, F., Cheng, C.-Y., Peters, J., and Ishii, H., 2016. "aeromorph-heat-sealing inflatable shape-change materials for interaction design". In Proceedings of the 29th Annual Symposium on User Interface Software and Technology, pp. 121–132.

[33] Dureisseix, D., 2012. "An overview of mechanisms and patterns with origami". *International Journal of Space Structures,* **27**(1), pp. 1–14.

[34] Miura, K., 1989. "A note on intrinsic geometry of origami". *Research of Pattern Formation*, pp. 91–102.

[35] Butler, J., Bowen, L., Wilcox, E., Shrager, A., Frecker, M. I., von Lockette, P., Simpson, T. W., Lang, R. J., Howell, L. L., and Magleby, S. P., 2018. "A model for multi-input mechanical advantage in origami-based mechanisms". *Journal of Mechanisms and Robotics,* **10**(6).

[36] Acer Kalafat, M., Sevinc, H., Samankan, S., Altinkaynak, A., and Temel, Z., 2020. "A novel origami inspired delta mechanism with flat parallelogram joints". *Journal of Mechanisms and Robotics*, pp. 1–22.

List of figure captions

Fig. 1. The 2D geometric pattern for a Kirigami model made from a piece of paper with cuts.

Fig. 2. A partially folded configuration of the Kirigami model (a) and the kinematic equivalent (b) which is a special over-constrained 6R linkage, type-III reconfigurable Bennett plano-spherical linkage.

Fig. 3. Two distinct motion branches of the reconfigurable Bennett plano-spherical linkage. (a) Spherical 4R linkage with rotating center C, (b) Planar 4R linkage.

Fig. 4 The novel reconfigurable parallel mechanism consists of three hybrid limbs, each of which employs a Bennett.

Fig. 5. Top view (opposite direction of Z-axis) of the parallel manipulator at its transitory configuration.

Fig. 6. he motion branch of the reconfigurable parallel manipulator that implements 3-DOF spherical motion.

Fig. 7. The motion branch that the platform of the parallel manipulator implements 3 DOFs rotation and 2 DOFs translation.

Fig. 8. Kinematic diagram of the limb 1 of the reconfigurable parallel manipulator in its 6-DOF configuration.

Fig. 9. The foldable origami base, rectangular tile: (a) 2D crease pattern, (b) partially folded configuration with a bending angle around the axis O_1O_2.

Fig. 10. A prototype of the bending actuator: (a) active bending by inflating the airbag with the paper origami card folding along the axis O_1O_2, (b) opposite side of the inflated actuator with deformed thin polyurethane (TPU) fabric layer, (c) the actuator bent passively around the axis O_1O_2 while the airbag is vacuumed.

Fig. 11. A prototype of the reconfigurable parallel manipulator employs three foldable Bennett plano-spherical linkage with inflatable bending actuators. (a) 6-DOF parallel manipulator with the 6R linkages corresponding to Fig. 2, (b) the transitory configuration of the foldable Bennett plano-spherical linkage, (c) 3-DOF spherical motion branch with the subchains in spherical 4R branch (Fig. 3(a)), (d) 5-DOF motion branch of the parallel manipulator with the planar 4R linkages (Fig. 3(b)).

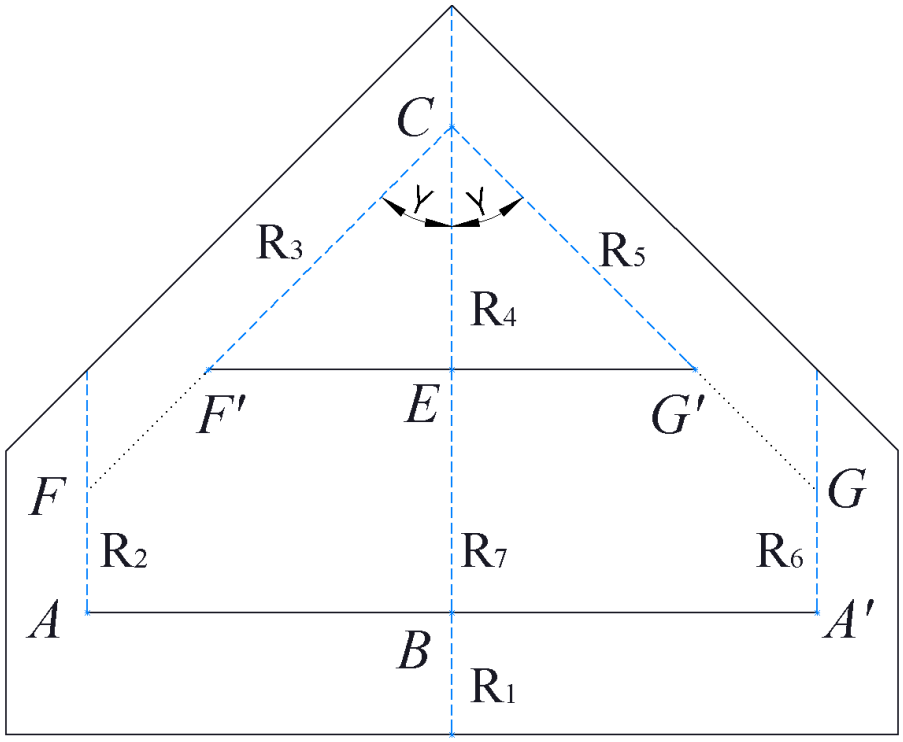

Fig. 1. The 2D geometric pattern for a Kirigami model made from a piece of paper with cuts.

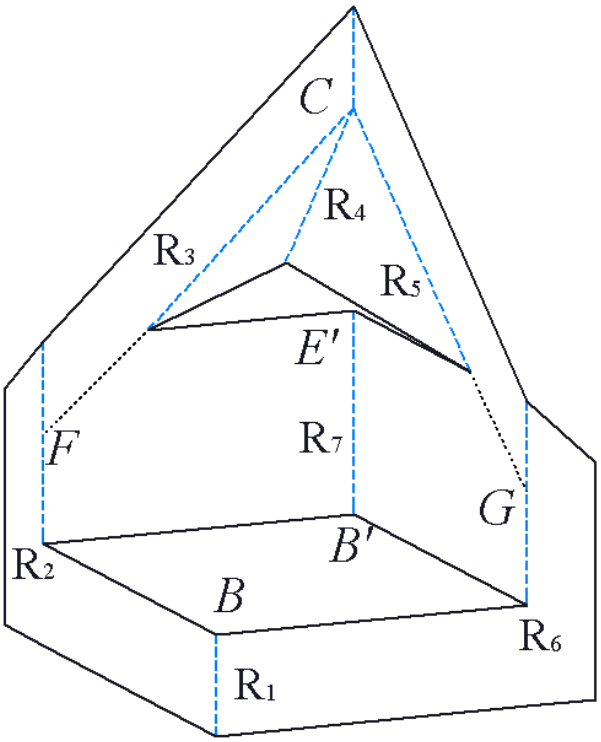

(a)

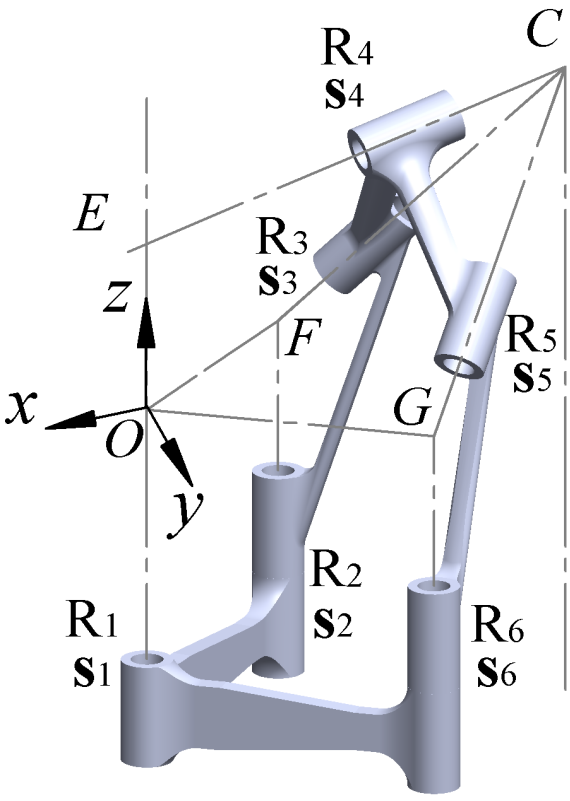

(b)

Fig. 2. A partially folded configuration of the Kirigami model (a) and the kinematic equivalent (b) which is a special overconstrained 6R linkage, type-III reconfigurable Bennett plano-spherical linkage.

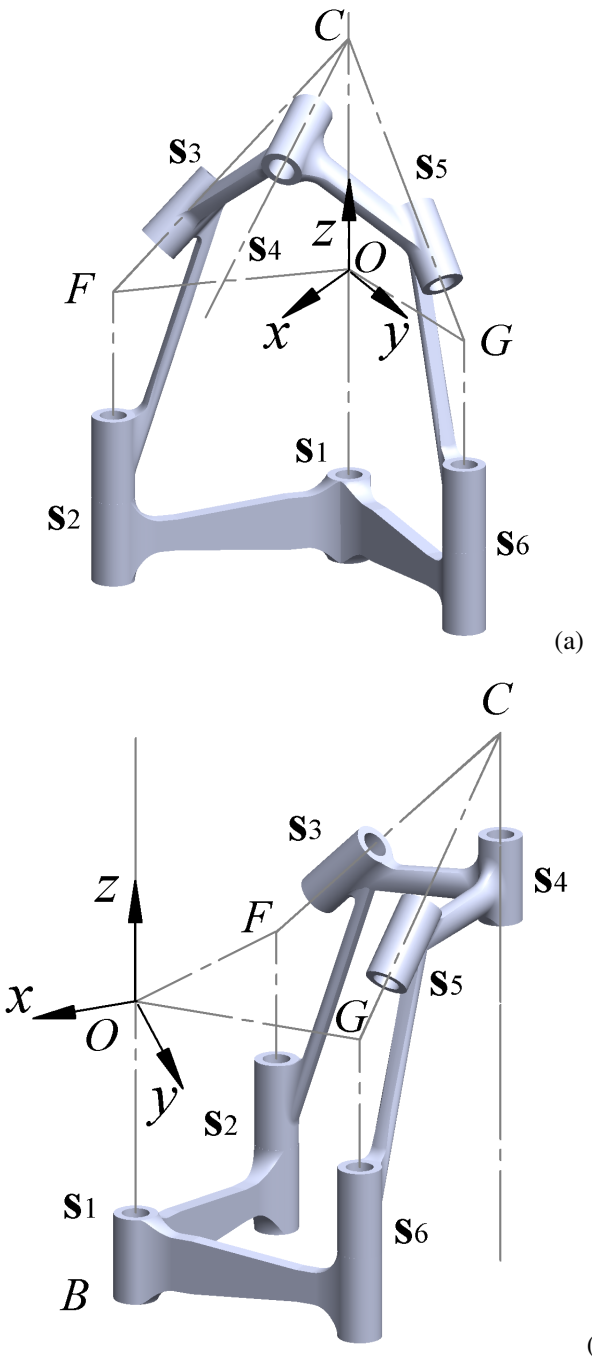

Fig. 3. Two distinct motion branches of the reconfigurable Bennett plano-spherical linkage. (a) Spherical 4R linkage with rotating center C, (b) Planar 4R linkage.

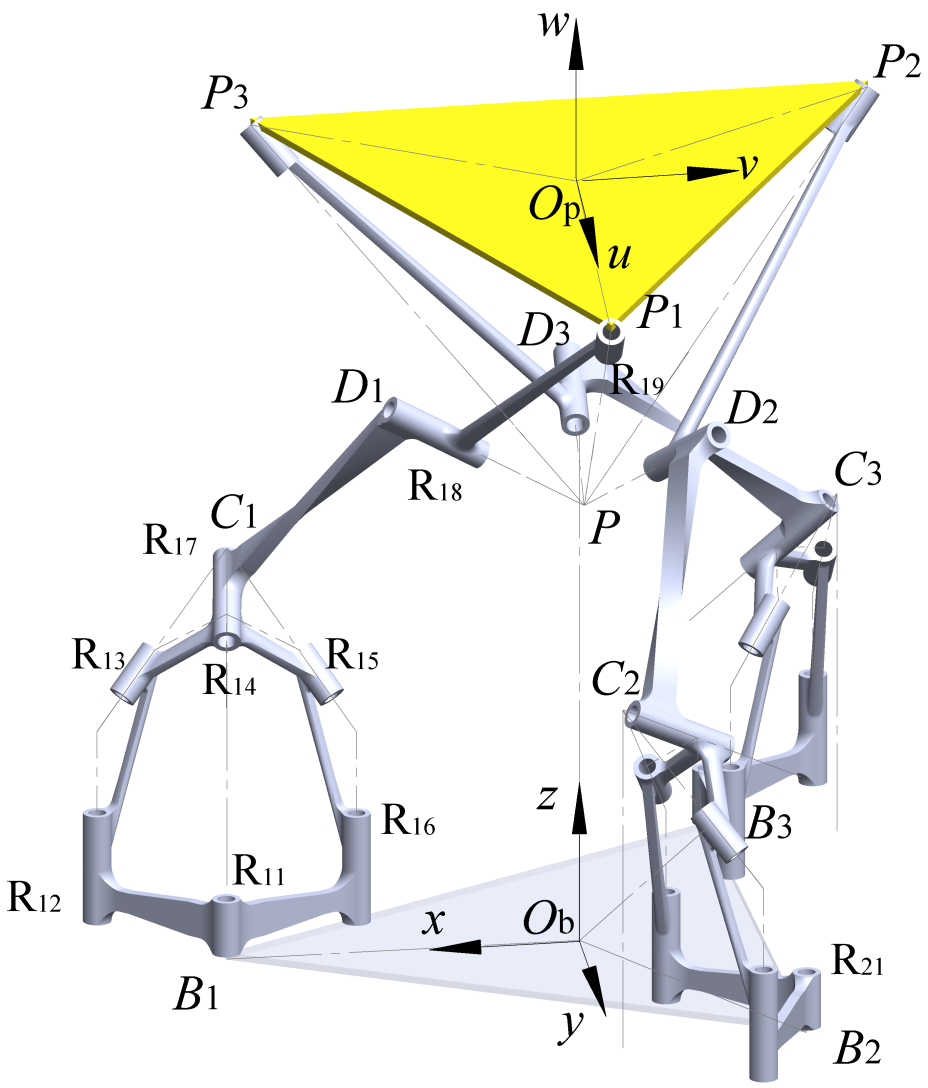

Fig. 4. The novel reconfigurable parallel mechanism consists of three hybrid limbs, each of which employs a Bennett plano-spherical linkage as subchain.

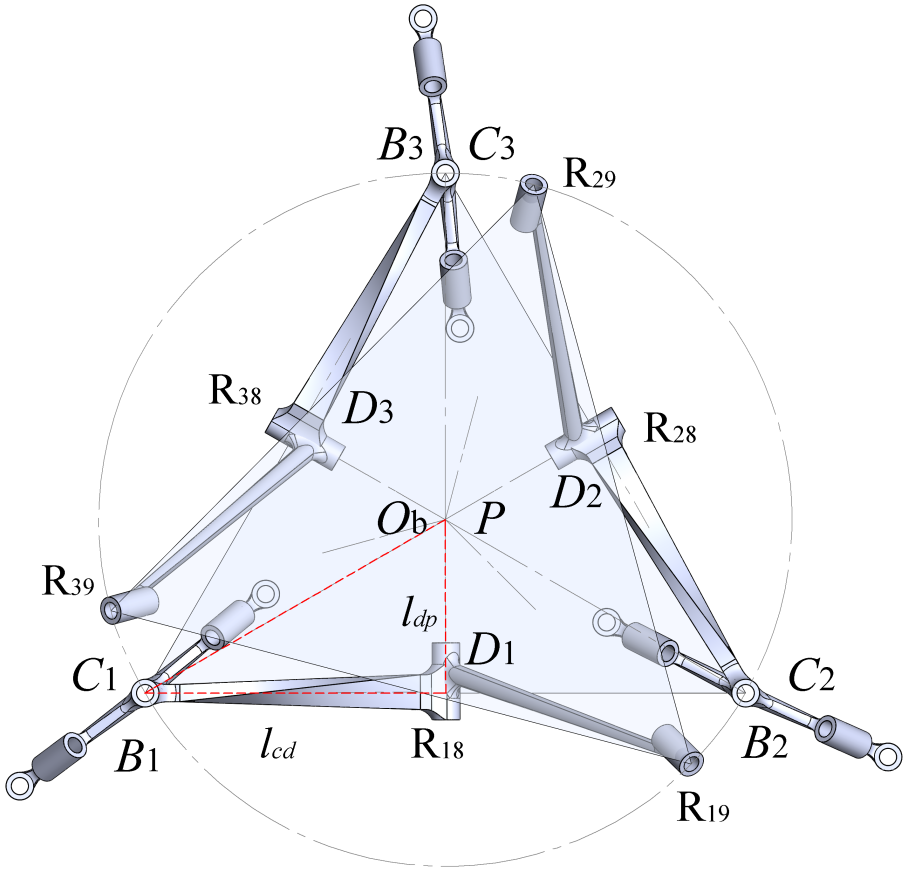

Fig. 5. Top view (opposite direction of Z-axis) of the parallel manipulator at its transitory configuration.

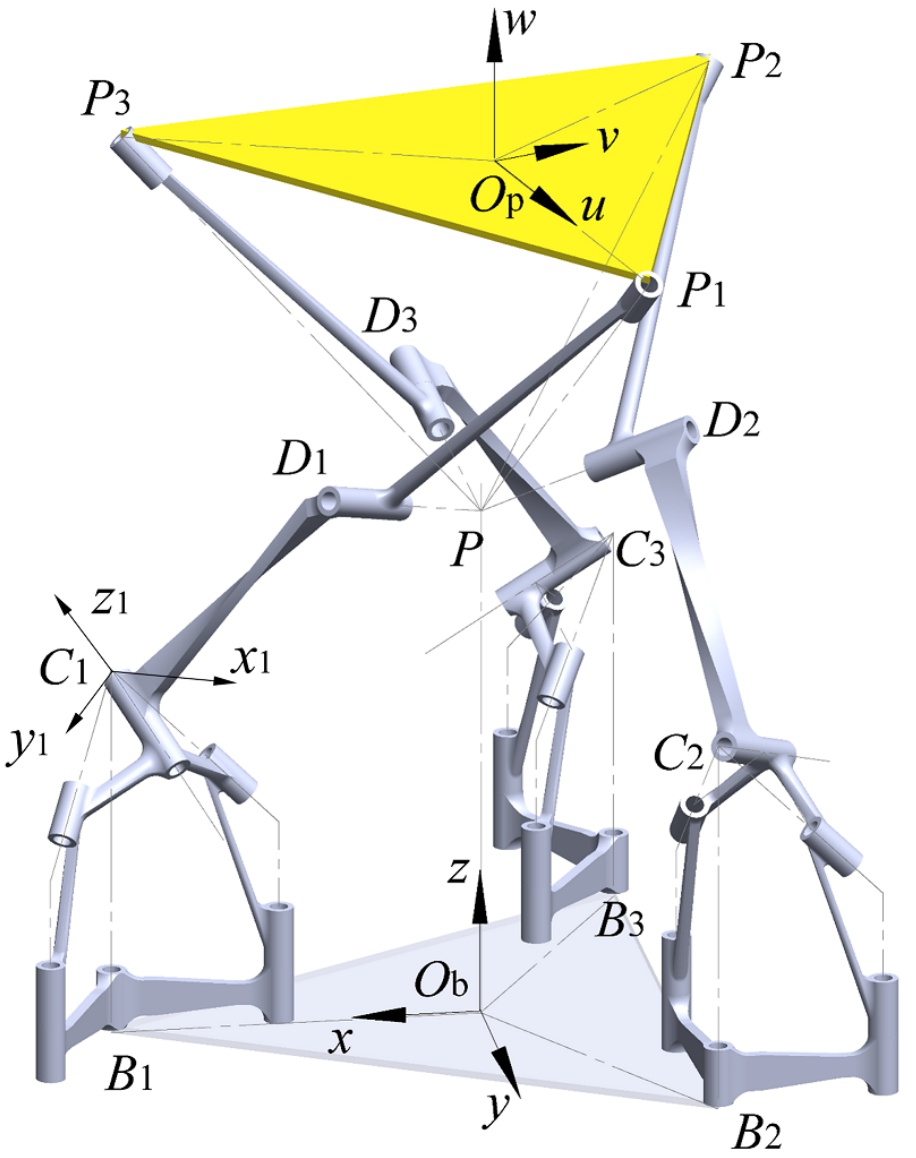

Fig. 6. The motion branch of the reconfigurable parallel manipulator that implements 3-DOF spherical motion.

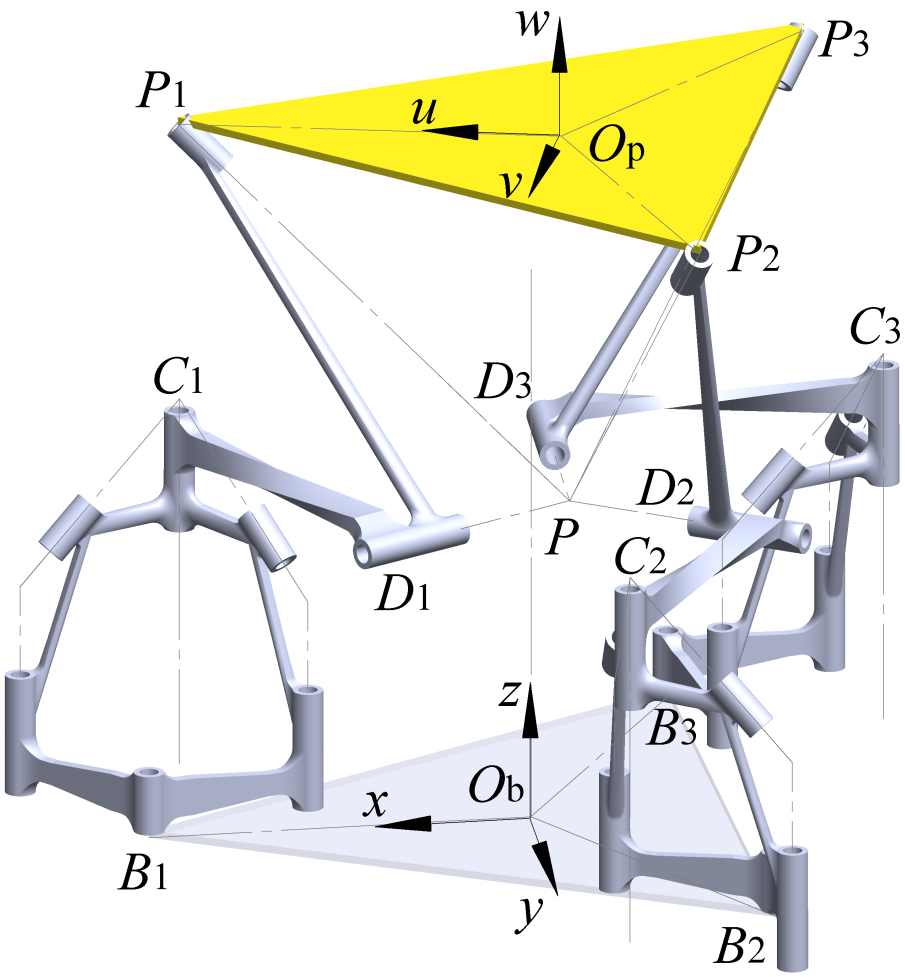

Fig. 7. The motion branch that the platform of the parallel manipulator implements 3 DOFs rotation and 2 DOFs translation.

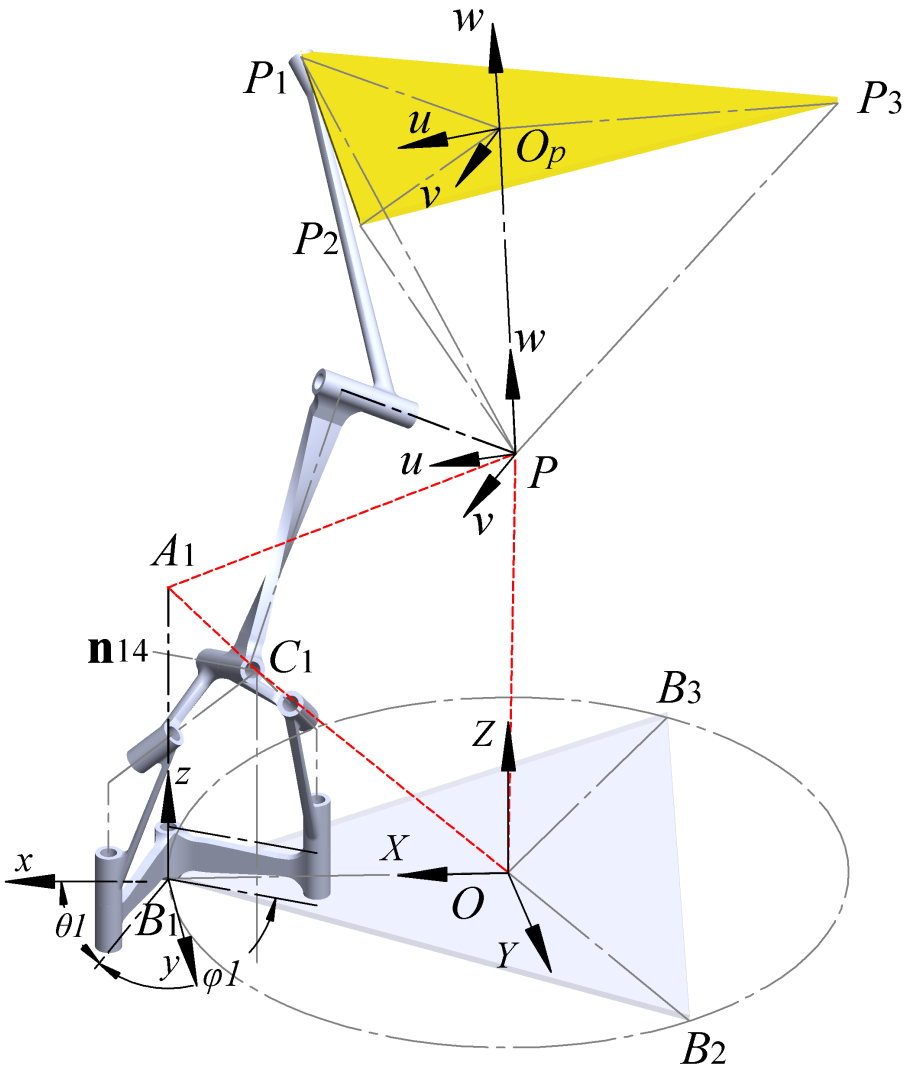

Fig. 8. Kinematic diagram of the limb 1 of the reconfigurable parallel manipulator in its 6-DOF configuration.

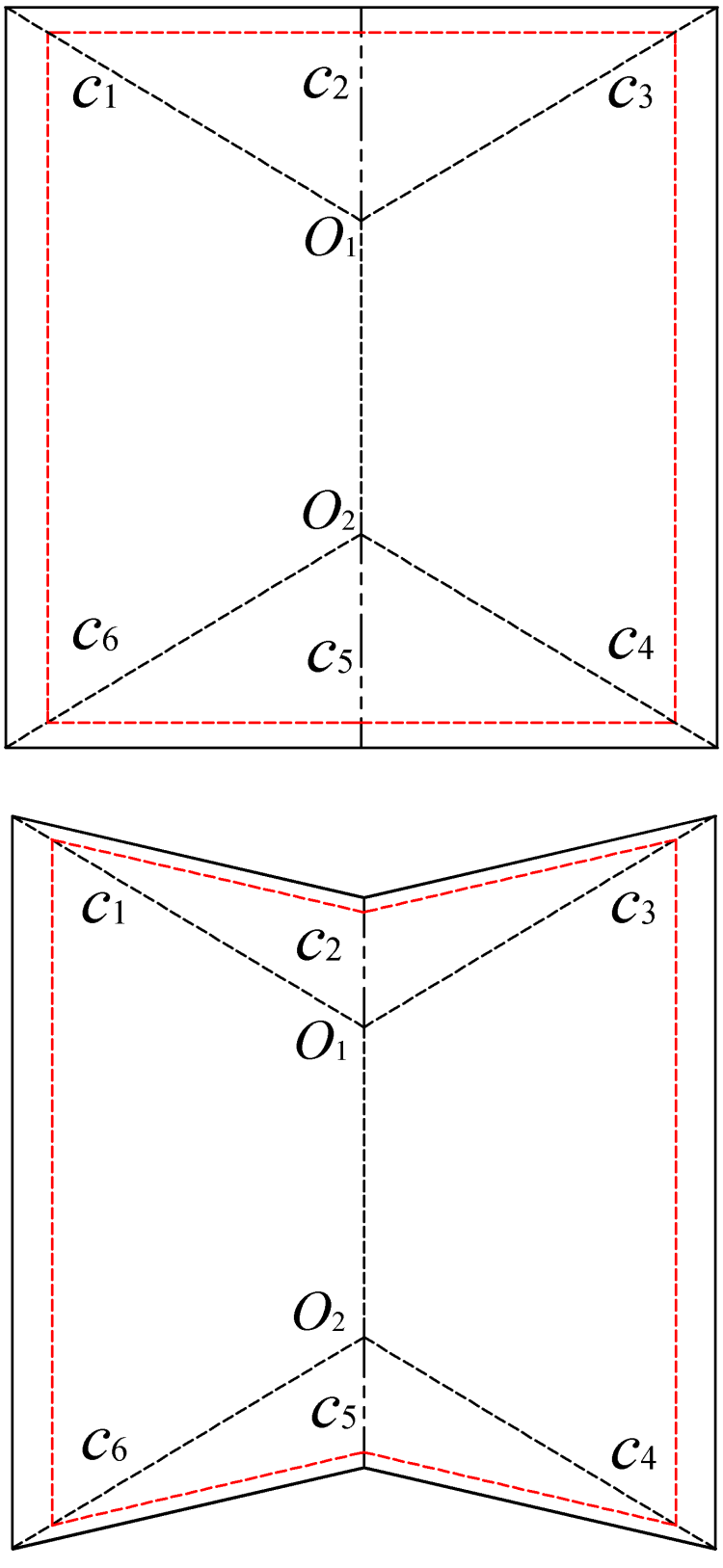

Fig. 9. The foldable origami base, rectangular tile: (a) 2D crease pattern, (b) partially folded configuration with a bending angle around the axis O_1O_2.

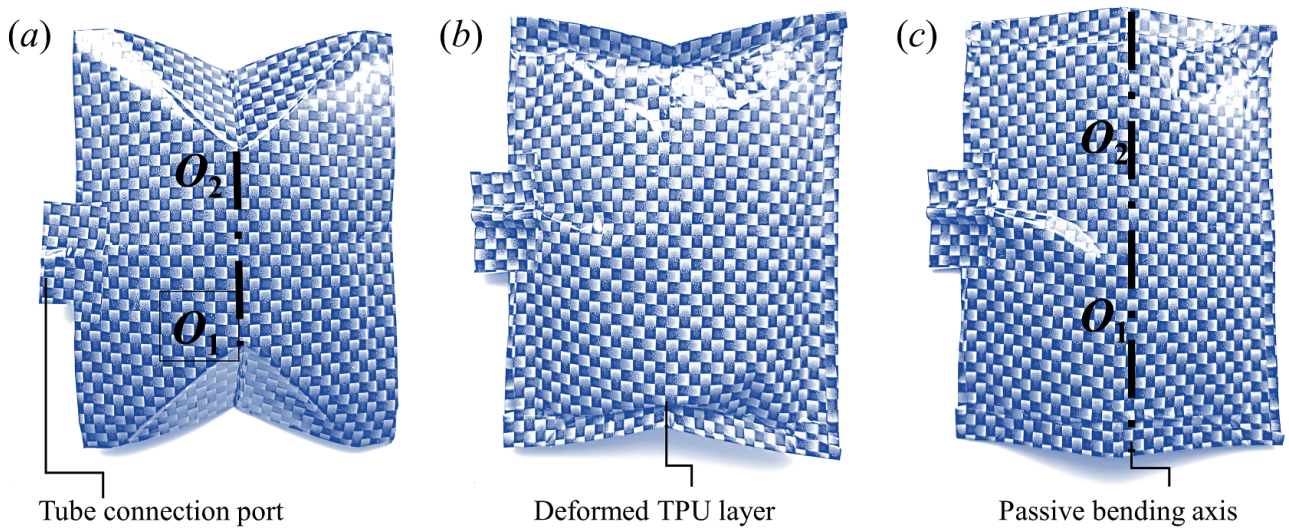

Fig. 10. A prototype of the bending actuator: (a) active bending by inflating the airbag with the paper origami card folding along the axis O_1O_2, (b) opposite side of the inflated actuator with deformed thin polyurethane (TPU) fabric layer, (c) the actuator bent passively around the axis O_1O_2 while the airbag is vacuumed.

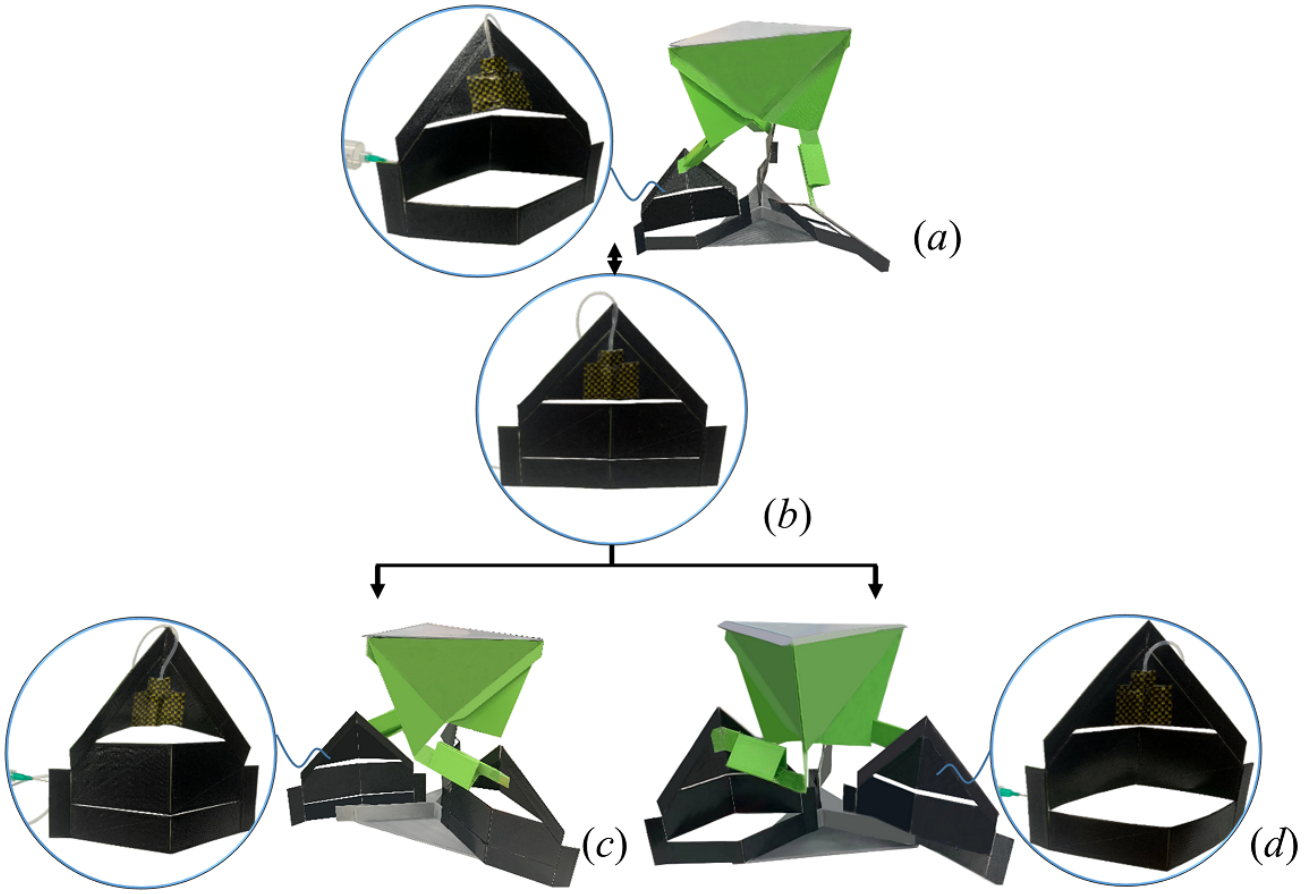

Fig. 11. A prototype of the reconfigurable parallel manipulator employs three foldable Bennett plano-spherical linkage with inflatable bending actuators. (a) 6-DOF parallel manipulator with the 6R linkages corresponding to Fig. 2, (b) the transitory configuration of the foldable Bennett plano-spherical linkage, (c) 3-DOF spherical motion branch with the subchains in spherical 4R branch (Fig. 3(a)), (d) 5-DOF motion branch of the parallel manipulator with the planar 4R linkages (Fig. 3(b)).